remote sensing

MDPI

Article

Optimizing Geo-Hazard Response: LBE-YOLO's Innovative Lightweight Framework for Enhanced Real-Time Landslide Detection and Risk Mitigation

Yingjie Du [1,2], Xiangyang Xu [1,*] and Xuhui He [3]

[1] The School of Rail Transit, Soochow University, Suzhou 215006, China; 0721211013@tute.edu.cn
[2] School of Automotive and Transportation, Tianjin University of Technology and Education, Tianjin 300222, China
[3] School of Civil Engineering, Central South University, Changsha 410075, China; xuhuihe@csu.edu.cn
* Correspondence: x.y.xu@suda.edu.cn; Tel.: +86-159-6219-8849

Abstract: Prompt detection of landslides is crucial for reducing the disaster risk and preventing landslides. However, landslide detection in practical applications still faces many challenges, such as the complexity of environmental backgrounds, the diversity of target scales, and the enormity of model weights. To address these issues, this paper proposes a lightweight LBE-YOLO model for real-time landslide detection. Firstly, a lightweight model is designed by integrating the GhostConv lightweight network with the YOLOv8n model. Inspired by GhostConv, this study innovatively designed the GhostC2f structure, which leverages linear thinking to further reduce the model parameters and computational burden. Additionally, the newly designed EGC2f structure, incorporating an attention mechanism, not only maintains the model's lightweight characteristics but also enhances the network's capability to extract valid information. Subsequently, the Path Aggregation Network (PAN) was optimized by introducing a bidirectional feature propagation mechanism to improve the model's feature fusion ability. Additionally, the Bijie landslide dataset was expanded through data augmentation strategies, thereby further improving the model's generalization capability. The experimental results indicate that, compared to the YOLOv8n model, the proposed model increased accuracy by 4.2%, while the model's weight and computational load were reduced by 32.0% and 35.5%, respectively. This verifies the superiority of the LBE-YOLO model in landslide target detection, which will help mitigate the impacts of natural disasters.

Keywords: attention mechanism; landslide detection; feature fusion; GhostConv; YOLOv8n

Citation: Du, Y.; Xu, X.; He, X. Optimizing Geo-Hazard Response: LBE-YOLO's Innovative Lightweight Framework for Enhanced Real-Time Landslide Detection and Risk Mitigation. *Remote Sens.* **2024**, *16*, 534. https://doi.org/10.3390/rs16030534

Academic Editor: Sandro Moretti

Received: 1 October 2023
Revised: 11 January 2024
Accepted: 29 January 2024
Published: 31 January 2024

1. Introduction

Landslides are a widespread and highly destructive natural disaster [1,2]. They present a significant global threat to both human society and the ecological environment [3]. These events lead to extensive land damage, substantial financial losses, and a significant loss of human lives [4,5]. Furthermore, several factors contribute to the increased frequency and severity of landslides. These factors include global climate change, population growth in mountainous regions, urbanization, and various human activities, like road construction and infrastructure development [6–8]. These elements have notably heightened the landslide risk. Hence, early detection of landslides has become an urgent priority within monitoring efforts. It plays a crucial role in mitigating their adverse impacts [9,10].

Previous landslide detection methods can be mainly divided into those based on geological surveying and seismic monitoring [11–13], and those based on computer vision [14–17]. Geological surveying involves specialized geological engineers conducting field surveys and observing topography, soil types, rock structures, and groundwater levels, among other factors, to assess the potential risk of landslides [18]. On the other

hand, due to the certain correlation between seismic activity and landslides, seismic monitoring is also used to detect potential landslide risks, especially in identifying precursors to landslides [19]. Utilizing seismographic equipment, the magnitude, depth of focus, and propagation of seismic waves can be measured to determine the relationship between seismic activity and the landslide risk [20]. Hong et al. [21] utilized the Frequency Ratio (FR), Certainty Factor (CF), and Index of Entropy (IOE) methods to create three groundbreaking models for assessing landslide susceptibility. Tailored to evaluate the risk of rain-induced landslides, these models have shown remarkable performance and reliability across training and validation datasets. Concurrently, Medina et al. [22] developed the Fast Shallow Landslide Assessment Model (FSLAM), a physically based tool. The FSLAM's strength is its rapid and efficient evaluation of regional landslide susceptibility caused by rainfall, offering essential scientific insights for effective landslide risk management. However, these traditional methods require expensive equipment, specialized technology, and substantial human resources, which to some extent limits their application in certain areas, especially in some developing countries. Moreover, due to the lack of real-time capabilities of these methods, their utility in emergency situations is constrained. Therefore, landslide real-time detection methods based on computer vision have been widely adopted [23–25].

In the initial phases, conventional machine learning approaches predominantly hinged on feature engineering to isolate landslide-related features, subsequently integrating them with suitable learning models to facilitate landslide identification [26–30]. Dou et al. [31] employed the Support Vector Machine (SVM) for predicting landslide types, demonstrating through experimental results that the average training and testing accuracies were 89.2% and 77.8%, respectively. Additionally, they discovered that the overall accuracy of the SVM did not exhibit a significant decrease concomitant with a reduction in the number of training samples. In a separate study, Chen et al. [32] utilized the Random Forest algorithm, achieving not only an enhancement of the classification accuracy through feature selection but also a reduction in the feature set, thereby yielding practical information pertinent to landslide identification. In addition, Selamat et al. [33] applied machine learning to the study of developing predictive models using an artificial neural network (ANN) to adequately evaluate the appropriate sampling rate for the Leng Yueh River Basin (LRB) model. However, these methods mainly depend on manual selection and feature engineering to determine the feature set, which not only relies on expert knowledge and has a high time cost but also may not necessarily pinpoint the optimal set of features. Therefore, deep learning techniques, capable of automatically extracting higher-level feature representations from raw data, have begun to be applied to handle complex landslide data [34–36].

The persistent advancement of deep learning has rendered landslides in various regions a focal point of research inquiry [37–42]. Yu et al. [43] employed Convolutional Neural Networks (CNNs) in conjunction with an optimized Region Growing Algorithm (RSG_R) to detect landslides. The team trained the CNN model using a dataset comprising images of landslides and subsequently extracted pivotal information, including the landslide area and boundaries, utilizing the RSG_R algorithm. This approach resulted in elevated detection accuracy. Despite the prevalent application of Convolutional Neural Networks (CNNs) for image classification tasks, they typically fall short of furnishing precise bounding box information for objects. This shortfall, when amalgamated with the considerable disparities in the dimensions and proportions of landslides, may culminate in either the omission of certain landslides or inaccurate detections.

In two-stage object detection methodologies, the initial phase involves the generation of candidate target regions [44]. Subsequently, a detailed detection, along with a bounding box regression, is performed on these areas in the second stage. This two-step process is pivotal for pinpointing targets accurately in landslide identification. To detect landslides, Yun et al. [45] introduced an optimized version of the Mask R-CNN model, which is predicated on the masked region. The model attains optimization through the incorporation of attention modules, utilization of bottom-up channels, and the introduction of GA-

RPN. Experimental outcomes demonstrate that the model achieves an accuracy rate of 92.6%. Jin et al. [46] employed Faster R-CNN for landslide identification and detection, introducing an efficient algorithm named ERCA. The main goal of this algorithm is to use the adaptive soft threshold in deep learning to reduce the noise interference of the image background in complex environments, thereby enhancing the performance of the target detection algorithm in feature learning. Nevertheless, a notable downside of these methods is their high computational load. Both the training and inference phases exhibit relatively slow speeds, a limitation that is particularly impactful given the critical need for real-time performance in landslide detection. To address this, the single-stage YOLO model has been introduced [47]. Characteristically, it employs anchor boxes to predict both the position and the category of the target. The YOLO series models, compared to their two-stage counterparts, enable more rapid detection [48]. They facilitate object detection across the entire image simultaneously, obviating the need for additional steps to generate candidate areas, and thereby find extensive application in landslide detection. Guo et al. [49] have integrated SBAS-InSAR technology with the YOLO model to detect landslides in mountainous regions. Their findings indicate that this amalgamated approach augments the congruence between detection outcomes and reference imagery. However, the issue of enhancing performance while considering lightweighting was not addressed. Ji et al. [50] employed a strategy predicated on Convolutional Neural Networks (CNNs) for landslide identification from high-resolution optical satellite imagery. The incorporation of the attention mechanism enhances the CNNs' ability to effectively distinguish unique landslide features from the background, thereby markedly ameliorating the landslide recognition performance. Li et al. [51] have refined the YOLOv4 model through the incorporation of MobileNetv3, depthwise separable convolution, and attention mechanisms, consequently improving the model's detection efficacy and speed. Nevertheless, the integration of multi-scale landslide targets was not contemplated in their work.

Consequently, this paper proposes a model termed LBE-YOLO, which strives to lighten the model while preserving the detection efficacy. The initial step involves the integration of the lightweight GhostConv network with the YOLOv8n architecture, thereby constructing a more lightweight model. Subsequently, an innovative GhostC2f structure is introduced, aiming to decrease the model's computational load further and achieve additional lightweighting. Additionally, a novel EGC2f structure is designed with the objective of enhancing the model's capacity for extracting pertinent information while concurrently reducing the model parameters. The Path Aggregation Network (PAN) is subsequently optimized to augment the model's proficiency in capturing target information across varying scales. Lastly, the Bijie landslide dataset is expanded through the employment of diverse data augmentation techniques—including random translation, adjustments of the brightness and saturation, and the introduction of noise—to elevate the model's generalization capability.

The remaining sections are structured as follows. The framework of the LBE-YOLO model is proposed in Section 2. Sections 3 and 4 present the experiment design and case study. Section 5 offers some thoughts on the findings.

2. Materials and Methods

2.1. Research Area and Dataset Establishment

The research area is in northwestern Guizhou Province, China, at latitudes 26°21′–27°46′N and longitudes 103°36′–106°43′E, covering all of Bijie City across about 26,853 square kilometers, as illustrated in Figure 1. Situated in the transitional zone between the Tibetan Plateau and the eastern hilly areas, the region is distinguished by its sloping terrain and unstable geological formations. It is notably characterized by a multitude of steep slopes, contributing significantly to the region's geological intricacy. It is a region transitioning from the Qinghai–Tibet Plateau to the eastern hills, featuring intricate terrain with numerous hills. The annual rainfall ranges from 849 to 1399 mm, making it one of China's most landslide-prone areas. Additionally, it experiences frequent new landslides, causing severe environmental damage. Given the challenges of on-site

investigations, it is crucial to develop efficient computer vision algorithms for early landslide warning, risk assessment, and post-disaster recovery, especially in emergencies.

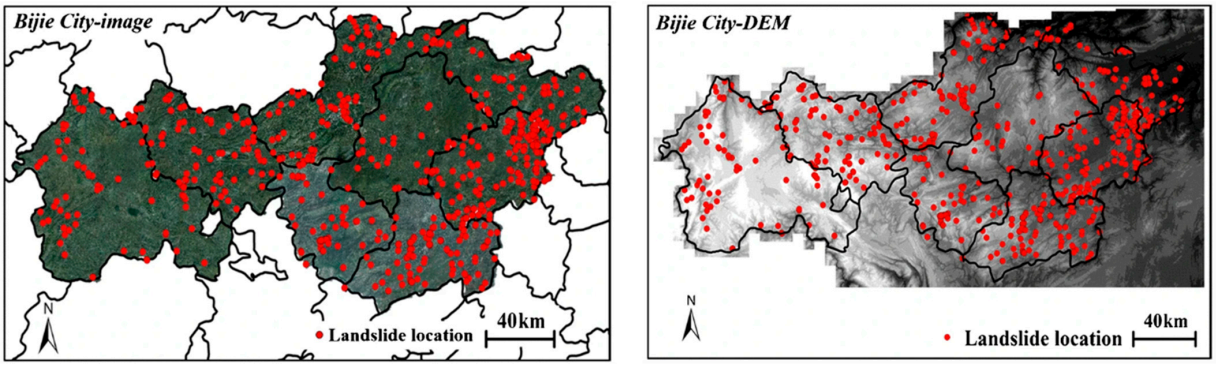

(**a**) (**b**)

Figure 1. Map of the Bijie research area. The locations of identified landslides are marked by red points. (**a**) The image of research area. (**b**) The DEM of research area [50].

To create a real-time landslide detection method, we conducted experiments using the Bijie landslide dataset. It includes 770 landslide samples, marked as red dots in Figure 1, representing actual landslide locations. To enhance the model's capacity for generalization, we expanded the dataset to 5770 images. Our data augmentation methods involved adjusting the brightness, adjusting saturation, adding noise, and random panning, as shown in Figure 2.

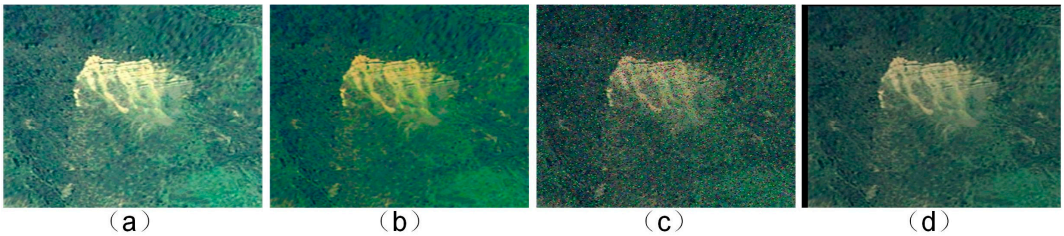

Figure 2. Data enhancement diagram: (**a**) adjusting brightness, (**b**) adjusting saturation, (**c**) adding noise, and (**d**) random panning.

To fulfill the requisites of the experiments, we randomly split the dataset into training and validation sets at an 8:2 ratio. We annotated the dataset using the Labeling tool, focusing on a single category, "landslide". The training set's label data include category information, central coordinates (x, y) of bounding boxes, width, and height measurements, all detailed in Figure 3.

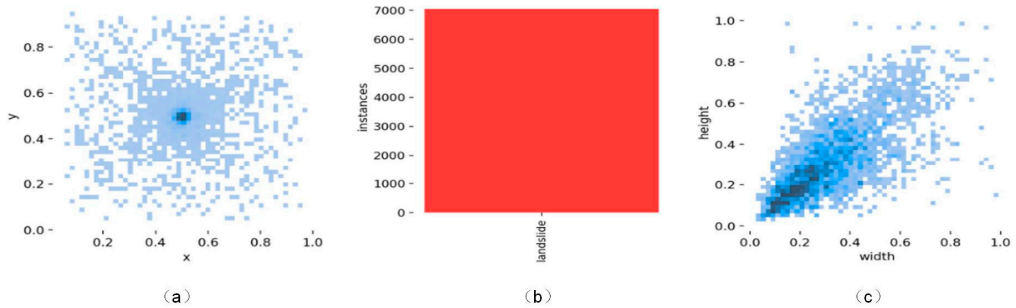

Figure 3. Label data volume and label distribution of landslides: (**a**) coordinates of the center point of the labeled box; (**b**) number of landslides; and (**c**) width and height distribution of the labeled boxes.

2.2. YOLOV8n Network Structure

YOLOv8 is the latest version in the YOLO series of object detection algorithms, consisting of four different network architectures: YOLOv8n, YOLOv8m, YOLOv8l, and YOLOv8x. As the model's depth increases, its detection performance gradually improves. Given the real-time requirements of landslide detection, we have chosen the lightweight YOLOv8n as the baseline model and optimized it. The YOLOv8n model is primarily divided into four parts: the input layer, the backbone layer, the neck layer, and the output layer, as shown in Figure 4.

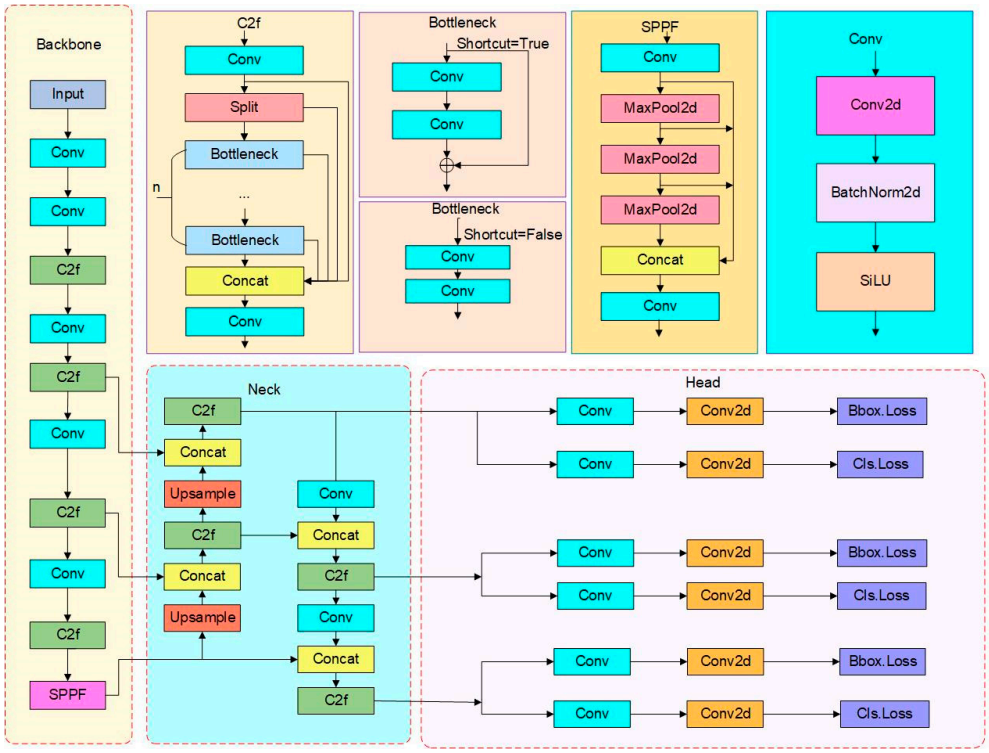

Figure 4. Structure of YOLOv8n.

The main task of the input layer is to perform various data augmentation operations on the input images, including scaling, adjusting hues, and applying Mosaic data augmentation, to adapt to the required training size. The core idea of the Mosaic data augmentation method is to randomly crop and scale four images, and then to concatenate them into one image for training data.

The backbone layer is responsible for extracting target features and consists of Conv, C2f, and SPPF modules. The Conv module performs convolution, batch normalization (BN), and SiLU activation function operations. The C2f module enhances the gradient propagation effectively by introducing more cross-layer branch connections, enriching the information flow of the feature extraction network. Unlike the SPP module in previous YOLO series, the SPPF module adopts three consecutive pooling operations, reducing the computational complexity while ensuring the fusion of multiscale information and an enlarged receptive field.

The neck layer's main role is feature integration across dimensions. It accomplishes this by effectively fusing feature maps from various levels using the FPN and PAN. This process accurately preserves spatial information, resulting in a significant enhancement of the network's detection performance.

The output layer is responsible for generating the final predictions of the object detection. It processes the refined feature maps provided by the neck structure and produces bounding box coordinates, class probabilities, and other relevant information for each

detected object. The output layer also applies non-maximum suppression (NMS) to filter out redundant detections and retain the most confident and accurate predictions. The final output is a set of bounding.

2.3. Improved YOLOV8n Network Structure

2.3.1. Lightweighting Improvement

In the process of landslide detection, enhancing the real-time accuracy of geological disaster monitoring is crucial for issuing warnings, reducing casualties, and minimizing property damage. However, the backbone network of the YOLOv8n model, aiming to expand the receptive field, extensively adopts convolution operations to increase the number of channels, thereby requiring more parameters and computational costs, adversely affecting real-time landslide detection. Hence, this paper employs GhostConv [52] for the lightweight processing of the YOLOv8n model's backbone network. The core principle of GhostConv is to generate feature maps using fewer base convolution kernels and subsequently produce additional Ghost feature maps through some low-cost operations, thereby improving the model's expressive capability without significantly increasing the computational burden, as illustrated in Figure 5.

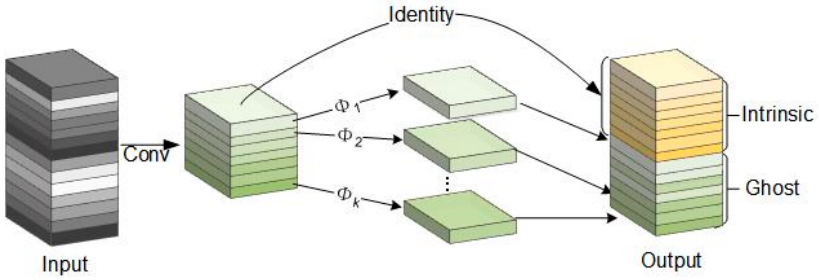

Figure 5. GhostConv's structure.

GhostBottleneck, designed based on GhostConv, is a lightweight structure. It primarily consists of two configurations, having strides of 1 and 2, respectively. The structure with a stride of 1 incorporates two 1 × 1 kernel GhostConvs. The initial GhostConv is tasked with expanding the channel number and bolstering the network's expressive capability. In contrast, the subsequent GhostConv restores the channel count, thereby maintaining consistency between the input and output feature maps. Residual connections integrated within this structure facilitate gradient backpropagation and sustain the network's expressive capacity, as depicted in Figure 6a.

In the GhostBottleneck structure with a stride of 2, an additional depthwise convolution is incorporated, based on the stride of 1 structure. Following the channel number expansion by the first GhostConv, the depthwise convolution initiates downsampling. Subsequently, the second GhostConv, in tandem with a 1 × 1 convolution, restores the channel number, ensuring consistency with the input. This innovative structure adeptly mitigates the computational demand and minimizes the gradient information loss. It achieves this while preserving the richness of the features through a harmonious integration of downsampling and channel number restoration, as further detailed in Figure 6b.

While the YOLOv8n model, aided by C2f, is proficient in extracting features from diverse feature map levels, the C2f structure is laden with multiple bottleneck layers, illustrated in Figure 3c. These bottlenecks encompass convolution kernels of assorted dimensions, such as 1 × 1 and 3 × 3. Despite facilitating the amalgamation and extraction of features across varied receptive fields, this composition precipitates an escalation in both the model parameters and computational intricacy, proving detrimental for real-time landslide detection applications. Consequently, drawing inspiration from GhostBottleneck, this study introduces a restructured GhostC2f to optimize the backbone's C2f structure, as showcased in Figure 7. In this innovative design, the C2f's bottleneck layers are supplanted by GhostBottleneck layers. This modification enables the network to access an enriched feature map array without

elevating the convolution computational load, thereby reducing the model complexity and parameter count, and ultimately, enhancing the operational efficiency.

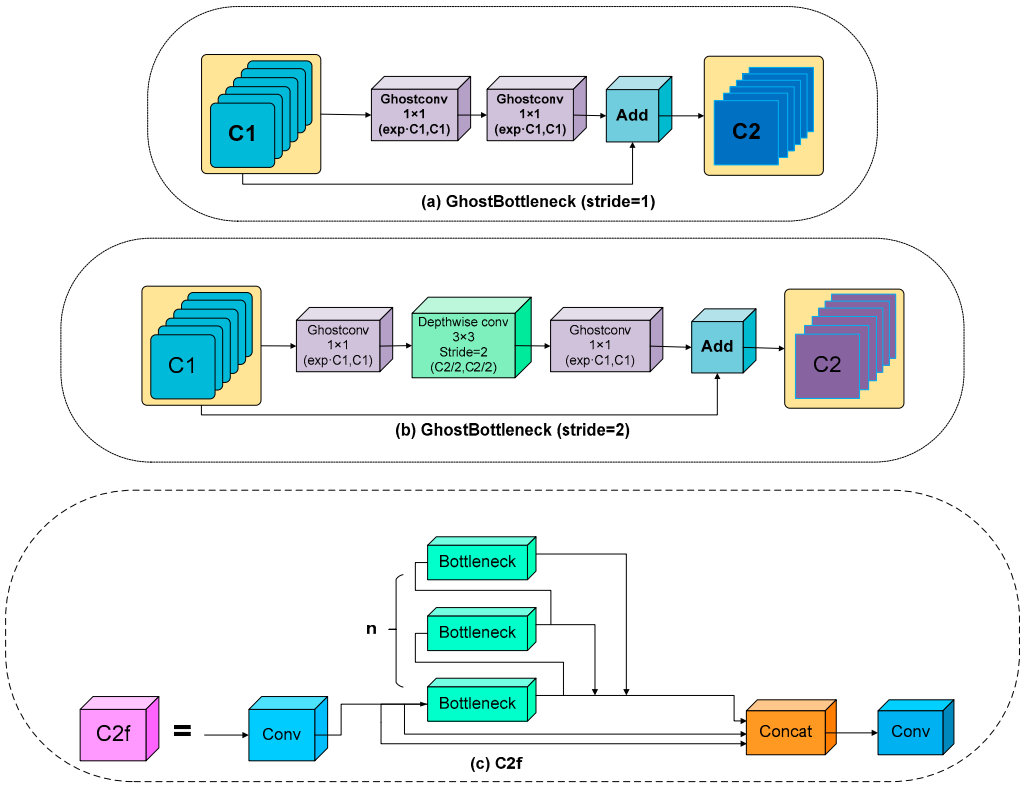

Figure 6. Two lightweight constructions and the C2f construction: (**a**) GhostBottleneck (stride = 1) construction; (**b**) GhostBottleneck (stride = 2) construction; and (**c**) C2f construction.

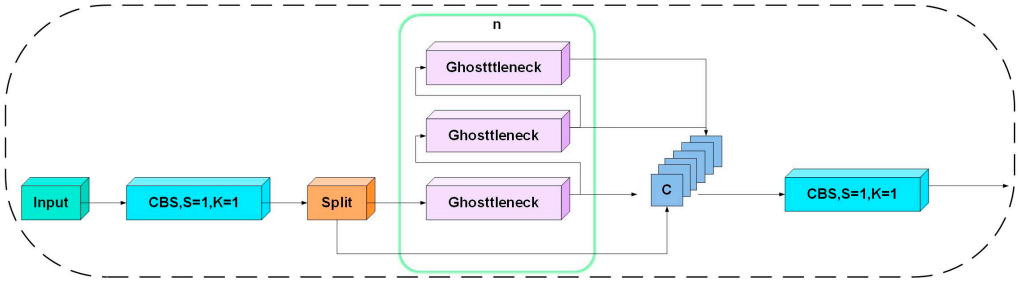

Figure 7. GhostC2f's structure.

2.3.2. Bidirectional Feature Pyramid Network (BiFPN)

In landslide detection processes, variations in the size and shape of landslides pose considerable challenges. YOLOv8n implements a strategy that melds the Feature Pyramid Network (FPN) and Path Aggregation Network (PAN) to amalgamate multi-scale feature information. This approach not only captures object information across various scales but also proficiently merges shallow high-resolution features with deep high-level semantic features. Nonetheless, this results in an augmentation of both the parameter count and computational load, while not fully accounting for the weight disparities among different input features. Consequently, this study introduces a Balanced Feature Pyramid Network (BIFPN) [53], depicted in Figure 8. This network realizes dynamic feature fusion through learnable weights instead of using simple feature concatenation or summation. This strategy enables the network to adjust the weights of each feature adaptively based on the task requirements, thereby achieving superior performance.

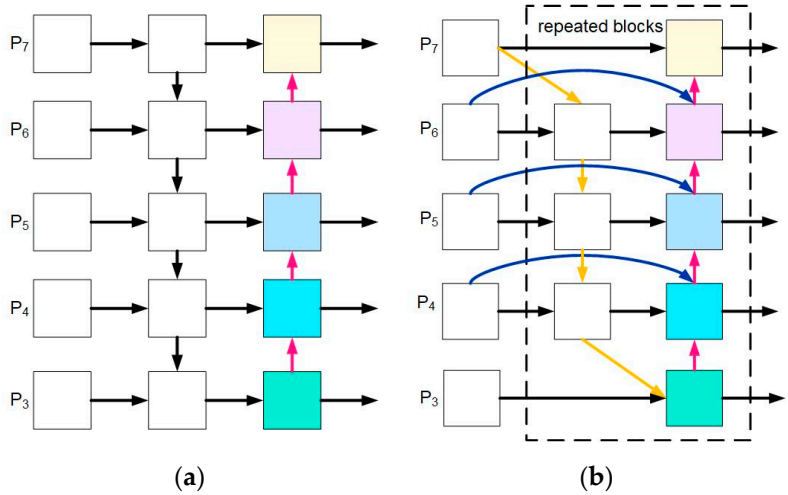

Figure 8. Structure diagram of the PAN and BiFPN: (**a**) structure of the PAN; and (**b**) structure of the BiFPN.

Initially, the BiFPN discards nodes with only a single input or output edge, given their relatively lower contributions to feature fusion. This strategy curtails the network's complexity, optimizing the architecture of the bidirectional network. Subsequently, the BiFPN incorporates skip connections between the initial input and output nodes. This inclusion facilitates cross-level feature fusion, thereby amplifying the accuracy of detection. In the final analysis, the network perceives a set of paths as a singular feature layer, realizing the fusion of more sophisticated features through multiple iterations, as shown in Figure 9.

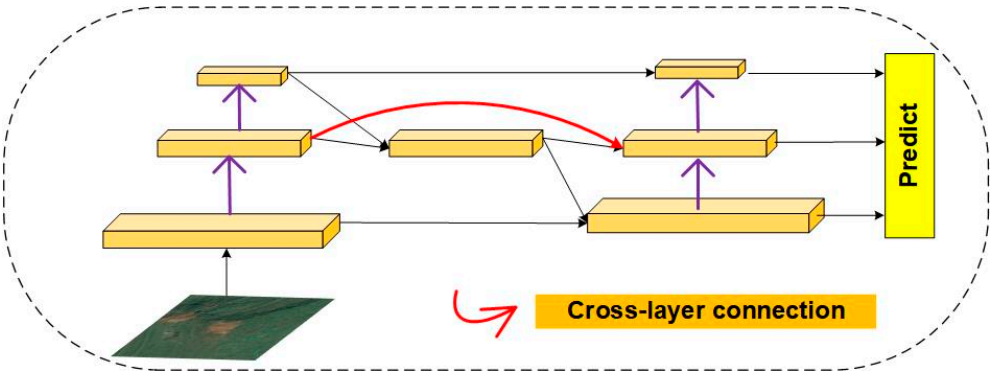

Figure 9. The BiFPN structure.

In addressing the diverse contributions from different resolution input features for landslide localization and classification, this study employs a swift normalization fusion method and introduces additional weights. This approach accomplishes feature fusion via dividing each weight by the cumulative sum of weights, enabling the network to discern the significance of each feature layer. Consequently, this results in enhanced performance in landslide detection tasks. The detailed calculation process is depicted in Equation (1):

$$O = \sum_i \frac{w_i}{\varepsilon + \sum_j w_j} \cdot I_i \tag{1}$$

where O denotes the output features, I_i represents the input features, and w signifies the node weights. It is noteworthy that the learning rate ε is set to 0.0001, with the purpose of preventing the generation of unstable outcomes.

2.3.3. EGC2f Structure

When faced with practical landslide detection, one often encounters a variety of complex detection backgrounds, which undoubtedly sets stricter standards for the accuracy of the landslide detection model. The YOLOv8n's neck layer employs the C2f structure, allowing for the amalgamation of multi-level, multi-scale semantic information through feature extraction, cross-layer connections, and integration. However, this design, while improving the detection performance, also escalates computational complexity and parameter count. Additionally, it does not fully address the channel dependence in the model output. Consequently, this study, drawing inspiration from the attention mechanism, integrates Efficient Channel Attention (ECA) [54] into the newly designed GhostC2f, culminating in the innovative EGC2f structure. Detailed in Figure 10, this structure enhances information extraction efficacy while maintaining a lightweight model.

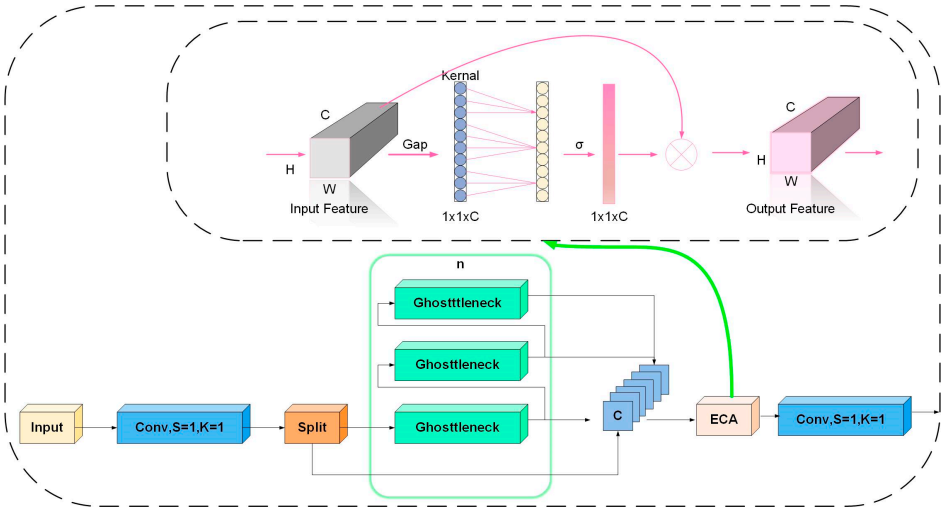

Figure 10. EGC2f's structure.

The SE attention mechanism relies on the compression of input features to achieve information extraction. However, this dimensionality reduction method may hinder the feature extraction ability during the convolution process. Therefore, the ECA (Efficient Channel Attention) module introduces a local cross-channel interaction strategy while keeping the dimensions unchanged, adding only a minimal number of model parameters but significantly improving performance. The ECA module first performs global average pooling on the input feature map, then applies a convolution kernel of size K to the pooled features for dimensionality reduction convolution, and finally calculates the weight information of each channel through the Sigmoid activation function. These weight pieces of information are multiplied element-wise with the original input feature map, eventually generating a feature map with channel attention. The adaptive function expression of the one-dimensional convolution of size k is shown in Equation (2):

$$K = \left| \frac{lb(C)}{\gamma} + \frac{b}{\gamma} \right|_{\text{odd}} \tag{2}$$

where C signifies the count of channels present in the input feature map. The parameter b is utilized to regulate the deviation in the convolution kernel size. Meanwhile, γ serves to modify the rate at which the size of the convolution kernel alters in correlation with the channel count. The notation $|\,|_{\text{odd}}$ denotes the proximity between k and the nearest odd number to the resultant value of the function.

2.4. Experimental Environment and Assessment Indicators

This study was executed within a Linux operating system, utilizing an Intel Xeon CPU E5-2680 v3 and an NVIDIA GeForce RTX 2080 Ti GPU with 11 GB VRAM. The PyTorch

1.7.0 framework and Python version 3.8 facilitated the execution. The experimental setup incorporated hyperparameters such as an initial learning rate of 0.01, a comprehensive 300 training epochs, and a batch size of 32.

To conduct a thorough assessment of the proposed model's efficacy in detecting landslides, this study employed four fundamental evaluation metrics: precision (P), recall (R), mean average precision (mAP), and $F1$. The corresponding computational formulas are presented below (refer to Equations (3)–(6)):

$$P = \frac{TP}{TP + FP} \tag{3}$$

$$R = \frac{TP}{TP + FN} \tag{4}$$

$$F1 = \frac{2 * P * R}{P + R} \tag{5}$$

$$mAP = \frac{\sum_{q=1}^{Q} AP(q)}{Q} \tag{6}$$

where precision quantifies the proportion of actual positive classes within the positive class predictions made by the model, whereas recall calculates the proportion of actual positive class samples accurately predicted. The mean average precision (mAP) represents the average of precision computed at various recall levels, serving as a comprehensive metric for model evaluation. The $F1$, the harmonic mean of precision and recall, is employed to holistically assess the model's accuracy and stability, providing a balanced view of the model performance [55,56].

To further evaluate the lightweight characteristics of the model, the following three core indicators are used: the number of parameters, the number of floating-point operations (FLOPs), and the size of the model weight file.

The parameters denote the learnable variables within the model, which are iteratively refined during training to minimize the model's loss. The FLOPs quantify the number of floating-point calculations achievable within a specific time frame, serving as a standard measure of a model's computational complexity or a particular operation's computational expense. The model weight file size indicates the model's intricacy and the storage space needed for its weights.

3. Experiments and Results

3.1. Results before and after Optimization

To validate the performance of the proposed LBE-YOLO model, we conducted a comparative validation with the sub-network YOLOv8n on the same validation dataset after training. The specific results are presented in Table 1.

Table 1. Comparison of the landslide detection results.

Model	Precision (%)	Recall (%)	F1 (%)	mAP (%)	Parameters (M)
YOLOv8n	86.4	85.8	86.0	87.7	3.01
LBE-YOLO	90.6	86.5	88.5	91.0	1.86

The data presented in Table 1 reveal a notable enhancement of the performance of the LBE-YOLO model over YOLOv8n across various metrics, including accuracy, recall rate, F1, mAP, and precision, registering improvements of 4.2%, 0.7%, 2.5%, and 3.3%, respectively. This marked superiority primarily stems from the refinement of the BiFPN architecture, bolstering the model's capability to amalgamate features at disparate levels. Furthermore, the incorporation of the novel ECA allows the model to concentrate more on pivotal features instrumental for landslide identification, thereby mitigating the

influence of inconsequential or disruptive features. Through the implementation of the innovatively crafted GhostC2f and EGC2f structures, LBE-YOLO has efficaciously diminished the parameter volume by 38.2%. This advancement is predominantly realized by alleviating the computational burden of actual convolution operations, consequently augmenting the model's operational efficiency. In essence, the model proposed herein attains a lightweight stature while preserving its detection efficacy, showcasing an augmented detection proficiency for landslide targets.

For a holistic assessment and juxtaposition of the model's efficacy in landslide detection before and after optimization, a comparative chart of the PR curve of the model, with an IOU value of 0.5 during the testing phase, was delineated, as depicted in Figure 11.

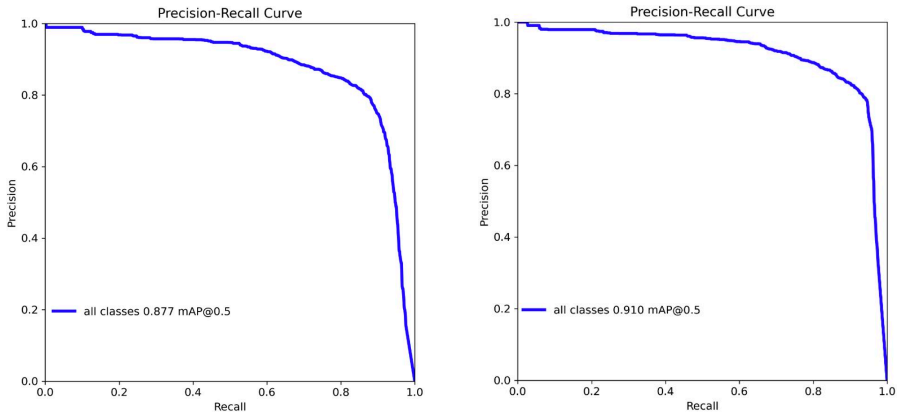

(**a**) (**b**)

Figure 11. PR diagram of YOLOv8n and LBE-YOLO: (**a**) YOLOv8n; and (**b**) LBE-YOLO.

The Area Under the Curve (AUC) serves as a pivotal metric for evaluating classification models; a larger AUC denotes superior model detection performance. Figure 11 unequivocally illustrates that the optimized model manifests enhanced detection capabilities.

3.2. Ablation Experiments

To demonstrate the effectiveness and lightweight characteristics of the LBE-YOLO network design, ablation experiments were conducted on the novel structure proposed in this study. The objective of this approach is to offer a clearer representation of the value embedded in each enhancement strategy. The relevant experimental results are illustrated in Figures 12 and 13 and Table 2.

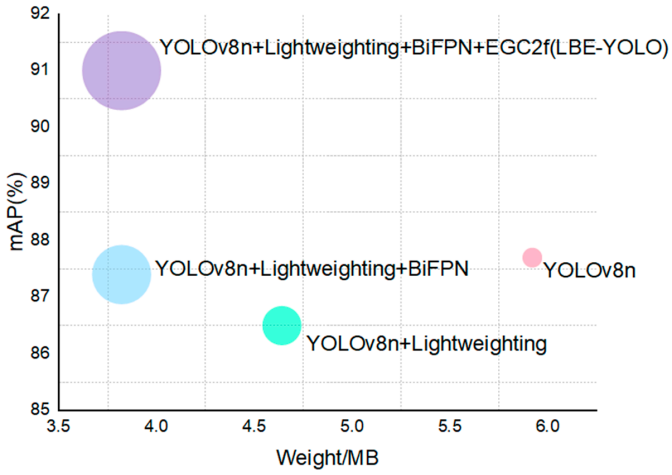

Figure 12. Comparison of the mAP with different model weights.

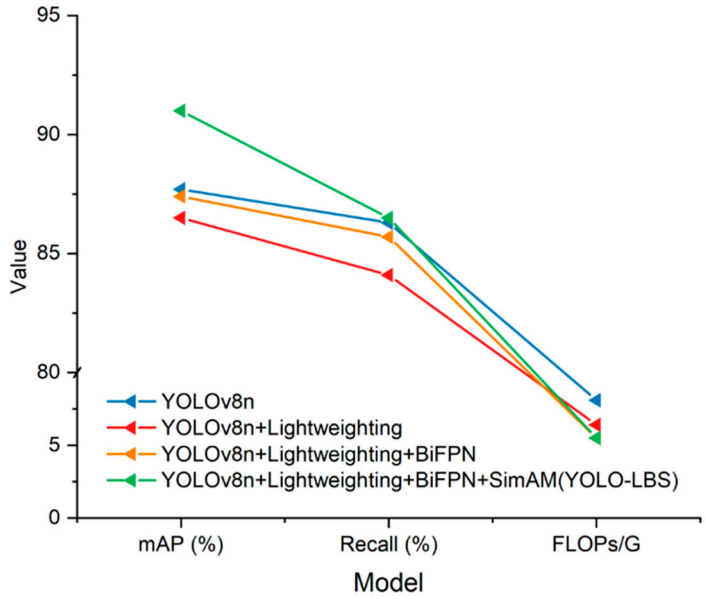

Figure 13. Comparison of the mAP with different models.

Table 2. Results of the ablation experiments.

Model	mAP (%)	Recall (%)	FLOPs/G	Weight/MB
YOLOv8n	87.7	86.3	8.1	5.92
YOLOv8n + Lightweighting	86.5	84.1	6.4	4.64
YOLOv8n + Lightweighting + BiFPN	87.4	85.7	5.5	3.82
YOLOv8n + Lightweighting + BiFPN + EGC2f (LBE-YOLO)	91.0	86.5	5.5	3.82

As illustrated in Table 2 and Figures 12 and 13, the integration of lightweight enhancements and the YOLOv8n sub-model resulted in a 32.0% and 35.5% reduction in the model's detection FLOP and weight, respectively. This outcome is primarily attributed to the significant reduction in the model's computational load facilitated by GhostConv, which substitutes certain convolution operations with more cost-efficient linear transformations, thereby optimizing the model's operational efficiency. Furthermore, this research introduced the innovative GhostC2f and EGC2f structures, contributing not only to a further decrease in the model's weight file size and computational demands but also to an augmentation of the model's expressive capacity.

Upon the enhancement of the BiFPN, the model experienced a notable increase of 0.9% in its mAP. This improvement is primarily attributed to the bidirectional information flow enabled by the BiFPN, ensuring efficient integration of features across multiple scales. As a result, the model can identify targets of varying scales with greater precision. Additionally, the incorporation of learnable weights is crucial to balancing the contributions of features at different levels, thereby enhancing the expressive capacity of the feature pyramid.

To elucidate the disparities in feature expression before and after the enhancement, feature maps from both model versions were visualized, as illustrated in Figure 14. An examination of the visualized results indicates that the feature maps generated by the BiFPN demonstrate superior globality and multi-scalability. This suggests that the feature maps contain a more diverse and rich set of information, significantly improving the model's ability to accurately detect and identify a wide range of complex and variable landslide features.

Upon the integration of the EGC2f structure, a significant enhancement was observed in the model's mAP value, marking a 3.6% increase. This improvement is primarily attributed to the incorporation of Efficient Channel Attention (ECA). ECA, by learning weights across various channels, can adaptively amplify the features of crucial channels while diminishing those of non-essential ones. This adaptability allows the model to

focus more on features beneficial to the task at hand. Additionally, ECA utilizes one-dimensional convolution for calculating the channel attention, effectively avoiding the high computational complexity associated with global self-attention, thereby enhancing the model's computational efficiency.

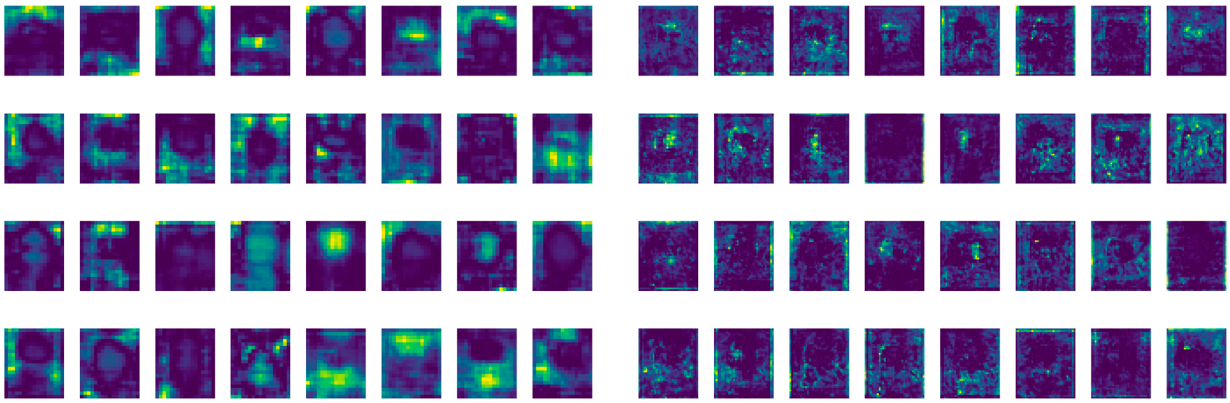

(**a**) (**b**)

Figure 14. Feature visualization maps: (**a**) YOLOv8n + Lightweighting; and (**b**) YOLOv8n + Lightweighting + BiFPN.

To empirically evaluate the impact of the introduced EGC2f structure on the model's performance, a Grad-CAM visualization analysis was conducted both before and after the structure's integration. An analysis of Figure 15 indicates that, following the incorporation of the EGC2f structure, the model demonstrates an improved concentration on accurate and relevant feature regions during classification or localization tasks. This refinement significantly boosts the model's detection efficacy for landslide targets across diverse scales.

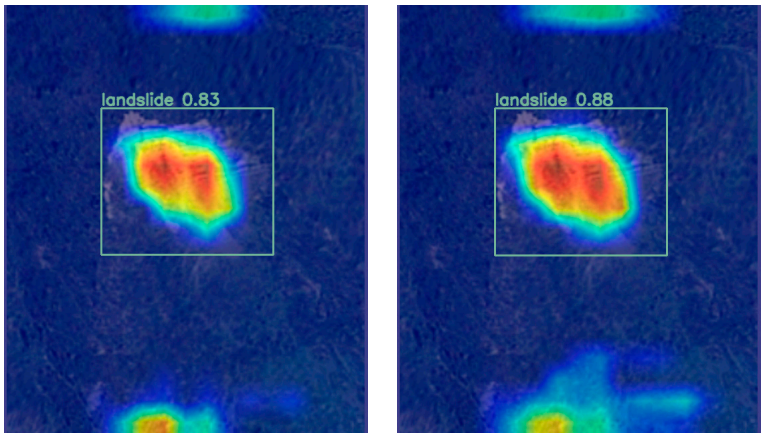

(**a**) (**b**)

Figure 15. Grad-CAM visualization: (**a**) YOLOv8n + Lightweighting + BiFPN; and (**b**) LBE-YOLO.

To elucidate the model's detection capabilities, multiple landslides were chosen for evaluation, the results of which are illustrated in Figure 16. In this figure, the detection outcomes are denoted by rectangular boxes, each accompanied by the corresponding category labels and associated confidence levels. It is evident that the LBE-YOLO model exhibits outstanding performance in identifying landslides, accurately discerning landslides of diverse scales with significant confidence.

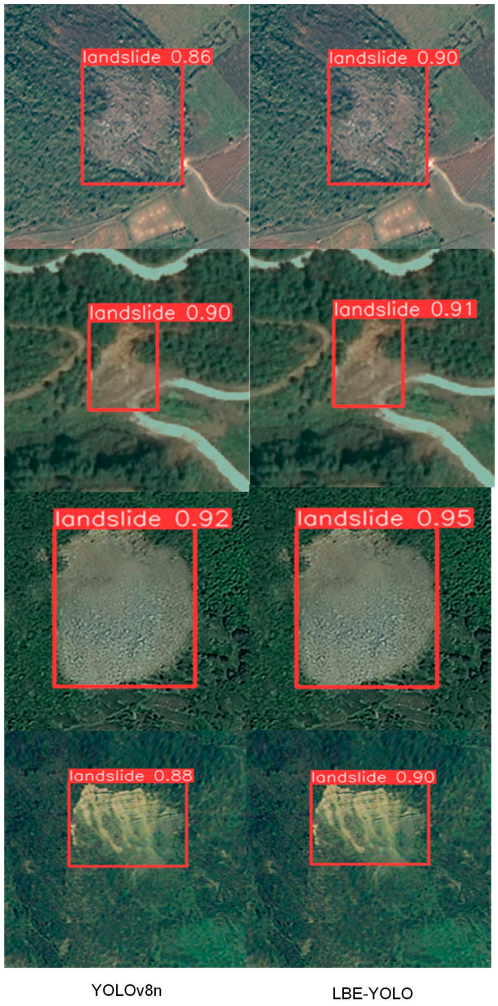

Figure 16. Test result figure.

3.3. Mainstream Algorithm Experiments

To assess the detection efficacy and lightweight features of the LBE-YOLO model, a comparative experimental analysis was conducted against both single-stage and two-stage mainstream object detection models. The outcomes of this comparative study are depicted in Figure 17 and Table 3.

Table 3 elucidates that the Faster R-CNN model exhibits a relatively diminished detection accuracy, predominantly attributed to its reliance on single-scale feature maps for generating anchor boxes. This attribute compromises its efficacy in detecting multi-scale objects in comparison to the alternative two-stage detection models. Additionally, the intricate network structure and substantial weight file size of the Faster R-CNN present obstacles for terminal deployment. As the network deepens, there is a concomitant reduction in the resolution of the feature map, thereby impairing the SSD model's proficiency in detecting smaller-scale objects, such as landslides. Conversely, YOLOv3-Tiny, while preserving the model lightweighting, employs feature maps of three distinct scales for the bounding box predictions, thereby improving the precision in locating landslides of various scales. YOLOv5, a progression from YOLOv3, has refined the loss function, guiding the model to focus on learning pivotal features during the training phase. This model also integrates a variety of data augmentation techniques, thereby enhancing the model's generalization capability. YOLOv7-Tiny, despite achieving lightweighting through a diminution in the model weights, witnesses a corresponding decrease in its capability for information extraction. The proposed LBE-YOLO model, while sustaining a lightweight framework, augments

its ability for valid information extraction and optimizes feature fusion for landslides of varying scales, ultimately leading to improved detection performance.

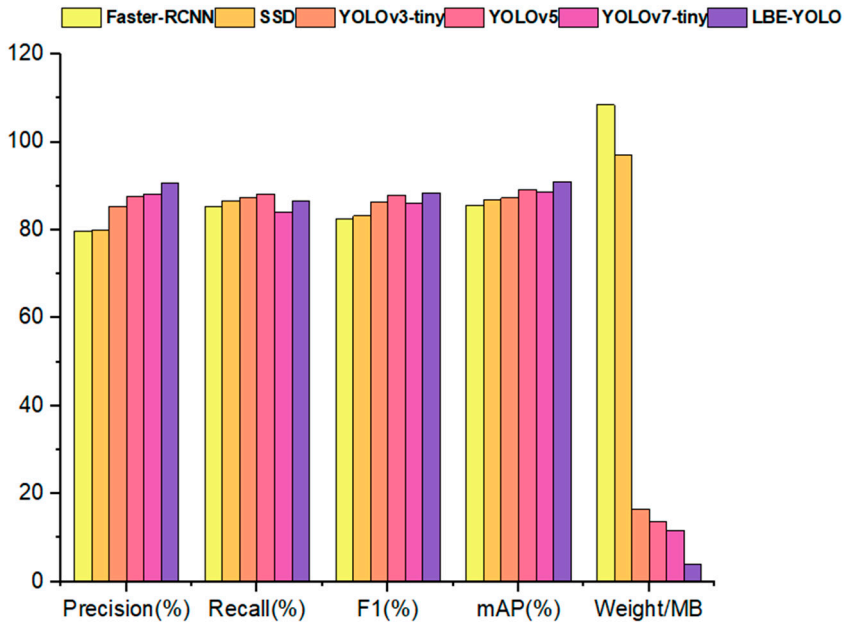

Figure 17. Comparison results with mainstream models.

Table 3. Comparison results with mainstream models.

Model	Precision (%)	Recall (%)	F1 (%)	mAP (%)	Weight/MB
Faster-RCNN	79.6	85.3	82.4	85.7	108.45
SSD	80.1	86.6	83.2	86.8	97.03
YOLOv3-tiny	85.3	87.5	86.4	87.3	16.46
YOLOv5	87.6	88.2	87.9	89.2	13.69
YOLOv7-tiny	88.2	84.0	86.0	88.6	11.67
LBE-YOLO	90.6	86.5	88.5	91.0	3.82

4. Discussion and Analysis

The timely identification of landslides holds paramount significance for issuing timely warnings and enacting emergency procedures to minimize damage. Accordingly, this manuscript presents an LBE-YOLO model designed specifically to strike a balance between optimal detection performance and model lightweighting. When compared to the YOLO series of detection models, it exhibits superior performance in landslide detection.

YOLOv8 stands as the most advanced model in the realm of single-stage object detection, demonstrating exceptional capabilities. However, the attainment of high performance with this model often necessitates significant computational resources, thereby posing challenges for its deployment on terminal devices. In light of this, the present study amalgamates the benefits derived from the GhostConv and YOLOv8n sub-models, thereby maintaining elevated performance levels while simultaneously reducing the computational and storage prerequisites. Furthermore, the introduction of a novel GhostC2f structure serves to optimize the standard convolution operations, resulting in a reduction in both the number of parameters and the computational expenditure. Simultaneously, an innovative EGC2f structure is devised, contributing to further model lightening and augmenting the extraction of pertinent information, which in turn enhances the detection performance. In addition, the refinement of the BiFPN enables the effective amalgamation of feature maps derived from varying levels, thereby improving the model's perceptibility for objects of diverse dimensions and proportions. The empirical data delineated in Tables 1–3 unequivocally showcase the exemplary performance of the proposed model in detecting landslides.

The data analysis from Experiment 3.3, presented in Table 3, indicates that the Faster-RCNN model has lower accuracy and that its significant model weight limits hardware deployment. Conversely, the SSD model shows higher detection accuracy but struggles to process uniquely shaped or sized targets due to its reliance on fixed-size anchor boxes during feature extraction. The YOLOv3-tiny model, with its straightforward architecture of stacked convolutional and pooling layers, substantially reduces both the network's parameters and the computational requirements. However, this reduction, resulting from fewer convolutional layers and filters, compromises its feature extraction efficiency, particularly impacting accuracy with targets of diverse sizes. In contrast, YOLOv5 enhances the feature extraction and information flow by integrating the PANet structure. This integration effectively combines features across various scales, thereby improving the detection of differently sized targets. The YOLOv7-tiny model, employing a combination of the ELAN and MaxPool2d structures, further boosts the feature extraction efficiency. Despite these improvements, the model's weight size remains considerably large. The LBE-YOLO model proposed in this paper not only enhances the detection performance and achieves model lightweighting but also strengthens the perception of targets at different scales. It can efficiently identify landslides in complex backgrounds, providing a new perspective for landslide detection.

Nonetheless, this study presents several limitations pertaining to the model optimization. The amalgamation of the GhostConv and YOLOv8n sub-models, complemented by the advent of the innovatively designed GhostC2f structure, has indeed mitigated the model's computational burden. However, this adaptation concurrently compromises its capability for information extraction. In the course of optimizing the Path Aggregation Network (PAN), the output garnered from the feature pyramid has not been fully harnessed, thereby signifying potential enhancements in detection performance. Moreover, the dataset employed in this research omits diverse and complex weather conditions such as nocturnal settings, torrential rain, heavy snowfall, and dense fog.

In the future, structures that balance detection performance and are lightweight will be designed to enhance landslide detection capabilities and optimize structures for better identification of landslides of different scales. At the same time, endeavors will be undertaken to diversify dataset types and broaden the range of scenarios encompassed, thereby bolstering the model's generalization proficiency.

5. Conclusions

This investigation introduces LBE-YOLO, a trailblazing deep learning methodology devised for the dynamic and effective identification of landslides via computational means. LBE-YOLO integrates two distinct sub-networks, namely GhostConv and YOLOv8n. GhostConv is instrumental in refining the network's architecture for efficiency, whereas YOLOv8n concentrates on global feature extraction. The novel introduction of the GhostC2f and EGC2f structures was aimed at both streamlining the model and enhancing its proficiency in capturing critical data. Furthermore, significant enhancements were implemented in the Path Aggregation Network (PAN) to advance the feature fusion processes. Empirical evidence attests to LBE-YOLO's eminent capability in detection, outstripping other prevalent object detection frameworks. Future endeavors will focus on advancing this model's efficiency, with an emphasis on elevating its detection prowess and exploring possibilities for its application in end-user devices.

Author Contributions: Conceptualization, Y.D. and X.X.; formal analysis, X.H.; methodology, Y.D. and X.X.; software, Y.D. and X.H.; validation, Y.D., X.X. and X.H.; writing—original draft, Y.D.; writing—review and editing, X.X. All authors have read and agreed to the published version of the manuscript.

Funding: This research was funded by the National Natural Science Foundation of China (No. 52308323, U1934209), Natural Science Foundation of Jiangsu Province, China (BK20220502) and Suzhou Innovation and Entrepreneurship Leading Talent Plan (No. ZXL2022488).

Data Availability Statement: The data used in this study can be obtained from the corresponding authors. The data are not publicly available due to laboratory results.

Acknowledgments: The authors would like to thank the editors and anonymous reviewers for their helpful suggestions.

Conflicts of Interest: The authors declare no conflicts of interest.

References

1. Yuan, C.; Li, Q.; Nie, W.; Ye, C. A Depth Information-Based Method to Enhance Rainfall-Induced Landslide Deformation Area Identification. *Measurement* **2023**, *219*, 113288. [CrossRef]
2. Ma, S.; Qiu, H.; Yang, D.; Wang, J.; Zhu, Y.; Tang, B.; Sun, K.; Cao, M. Surface Multi-Hazard Effect of Underground Coal Mining. *Landslides* **2023**, *20*, 39–52. [CrossRef]
3. Guzzetti, F.; Mondini, A.C.; Cardinali, M.; Fiorucci, F.; Santangelo, M.; Chang, K.-T. Landslide Inventory Maps: New Tools for an Old Problem. *Earth-Sci. Rev.* **2012**, *112*, 42–66. [CrossRef]
4. Bell, R.; Fort, M.; Götz, J.; Bernsteiner, H.; Andermann, C.; Etzlstorfer, J.; Posch, E.; Gurung, N.; Gurung, S. Major Geomorphic Events and Natural Hazards during Monsoonal Precipitation 2018 in the Kali Gandaki Valley, Nepal Himalaya. *Geomorphology* **2021**, *372*, 107451. [CrossRef]
5. Yin, H.; Zhang, G.; Wu, Q.; Yin, S.; Soltanian, M.R.; Thanh, H.V.; Dai, Z. A Deep Learning-Based Data-Driven Approach for Predicting Mining Water Inrush from Coal Seam Floor Using Microseismic Monitoring Data. *IEEE Trans. Geosci. Remote Sens.* **2023**, *61*, 1–15. [CrossRef]
6. Sun, W.; Tian, Y.; Mu, X.; Zhai, J.; Gao, P.; Zhao, G. Loess Landslide Inventory Map Based on GF-1 Satellite Imagery. *Remote Sens.* **2017**, *9*, 314. [CrossRef]
7. Ye, C.; Li, Y.; Cui, P.; Liang, L.; Pirasteh, S.; Marcato, J.; Goncalves, W.N.; Li, J. Landslide Detection of Hyperspectral Remote Sensing Data Based on Deep Learning with Constrains. *IEEE J. Sel. Top. Appl. Earth Obs. Remote Sens.* **2019**, *12*, 5047–5060. [CrossRef]
8. Cui, P.; Zhu, Y.; Han, Y.; Chen, X.; Zhuang, J. The 12 May Wenchuan Earthquake-Induced Landslide Lakes: Distribution and Preliminary Risk Evaluation. *Landslides* **2009**, *6*, 209–223. [CrossRef]
9. Zhou, G.; Li, W.; Zhou, X.; Tan, Y.; Lin, G.; Li, X.; Deng, R. An Innovative Echo Detection System with STM32 Gated and PMT Adjustable Gain for Airborne LiDAR. *Int. J. Remote Sens.* **2021**, *42*, 9187–9211. [CrossRef]
10. Yin, L.; Wang, L.; Li, J.; Lu, S.; Tian, J.; Yin, Z.; Liu, S.; Zheng, W. YOLOV4_CSPBi: Enhanced Land Target Detection Model. *Land* **2023**, *12*, 1813. [CrossRef]
11. Walter, F.; Burtin, A.; McArdell, B.W.; Hovius, N.; Weder, B.; Turowski, J.M. Testing Seismic Amplitude Source Location for Fast Debris-Flow Detection at Illgraben, Switzerland. *Nat. Hazards Earth Syst. Sci.* **2017**, *17*, 939–955. [CrossRef]
12. Manconi, A.; Picozzi, M.; Coviello, V.; De Santis, F.; Elia, L. Real-time Detection, Location, and Characterization of Rockslides Using Broadband Regional Seismic Networks. *Geophys. Res. Lett.* **2016**, *43*, 6960–6967. [CrossRef]
13. Yang, C.-M.; Kang, K.-H.; Yang, S.-H.; Li, K.-W.; Wang, H.-J.; Lee, Y.-T.; Lin, K.-K.; Pan, Y.-W.; Liao, J.-J. Large Paleo-Rockslide Induced by Buckling Failure at Jiasian inSouthern Taiwan. *Landslides* **2020**, *17*, 1319–1335. [CrossRef]
14. Yu, B.; Wang, N.; Xu, C.; Chen, F.; Wang, L. A Network for Landslide Detection Using Large-Area Remote Sensing Images with Multiple Spatial Resolutions. *Remote Sens.* **2022**, *14*, 5759. [CrossRef]
15. Sataer, G.; Sultan, M.; Emil, M.K.; Yellich, J.A.; Palaseanu-Lovejoy, M.; Becker, R.; Gebremichael, E.; Abdelmohsen, K. Remote Sensing Application for Landslide Detection, Monitoring along Eastern Lake Michigan (Miami Park, MI). *Remote Sens.* **2022**, *14*, 3474. [CrossRef]
16. Yu, B.; Xu, C.; Chen, F.; Wang, N.; Wang, L. HADeenNet: A Hierarchical-Attention Multi-Scale Deconvolution Network for Landslide Detection. *Int. J. Appl. Earth Obs. Geoinf.* **2022**, *111*, 102853. [CrossRef]
17. Mondini, A.C.; Guzzetti, F.; Melillo, M. Deep Learning Forecast of Rainfall-Induced Shallow Landslides. *Nat. Commun.* **2023**, *14*, 2466. [CrossRef]
18. Dong, J.-J.; Tung, Y.-H.; Chen, C.-C.; Liao, J.-J.; Pan, Y.-W. Discriminant Analysis of the Geomorphic Characteristics and Stability of Landslide Dams. *Geomorphology* **2009**, *110*, 162–171. [CrossRef]
19. Yang, C.-M.; Chang, J.-M.; Hung, C.-Y.; Lu, C.-H.; Chao, W.-A.; Kang, K.-H. Life Span of a Landslide Dam on Mountain Valley Caught on Seismic Signals and Its Possible Early Warnings. *Landslides* **2022**, *19*, 637–646. [CrossRef]
20. Chao, W.-A.; Zhao, L.; Chen, S.-C.; Wu, Y.-M.; Chen, C.-H.; Huang, H.-H. Seismology-Based Early Identification of Dam-Formation Landquake Events. *Sci. Rep.* **2016**, *6*, 19259. [CrossRef]
21. Hong, H.; Chen, W.; Xu, C.; Youssef, A.M.; Pradhan, B.; Tien Bui, D. Rainfall-Induced Landslide Susceptibility Assessment at the Chongren Area (China) Using Frequency Ratio, Certainty Factor, and Index of Entropy. *Geocarto Int.* **2017**, *32*, 139–154. [CrossRef]
22. Medina, V.; Hürlimann, M.; Guo, Z.; Lloret, A.; Vaunat, J. Fast Physically-Based Model for Rainfall-Induced Landslide Susceptibility Assessment at Regional Scale. *Catena* **2021**, *201*, 105213. [CrossRef]
23. Yang, D.; Qiu, H.; Ye, B.; Liu, Y.; Zhang, J.; Zhu, Y. Distribution and Recurrence of Warming-Induced Retrogressive Thaw Slumps on the Central Qinghai-Tibet Plateau. *JGR Earth Surf.* **2023**, *128*, e2022JF007047. [CrossRef]

24. Li, W.; Zhu, J.; Fu, L.; Zhu, Q.; Xie, Y.; Hu, Y. An Augmented Representation Method of Debris Flow Scenes to Improve Public Perception. *Int. J. Geogr. Inf. Sci.* **2021**, *35*, 1521–1544. [CrossRef]
25. Li, Q.; Song, D.; Yuan, C.; Nie, W. An Image Recognition Method for the Deformation Area of Open-Pit Rock Slopes under Variable Rainfall. *Measurement* **2022**, *188*, 110544. [CrossRef]
26. Pourghasemi, H.R.; Kerle, N. Random Forests and Evidential Belief Function-Based Landslide Susceptibility Assessment in Western Mazandaran Province, Iran. *Environ. Earth Sci.* **2016**, *75*, 185. [CrossRef]
27. Song, Y.; Gong, J.; Gao, S.; Wang, D.; Cui, T.; Li, Y.; Wei, B. Susceptibility Assessment of Earthquake-Induced Landslides Using Bayesian Network: A Case Study in Beichuan, China. *Comput. Geosci.* **2012**, *42*, 189–199. [CrossRef]
28. Sahin, E.K. Assessing the Predictive Capability of Ensemble Tree Methods for Landslide Susceptibility Mapping Using XGBoost, Gradient Boosting Machine, and Random Forest. *SN Appl. Sci.* **2020**, *2*, 1308. [CrossRef]
29. Sahin, E.K.; Colkesen, I.; Kavzoglu, T. A Comparative Assessment of Canonical Correlation Forest, Random Forest, Rotation Forest and Logistic Regression Methods for Landslide Susceptibility Mapping. *Geocarto Int.* **2020**, *35*, 341–363. [CrossRef]
30. Pham, B.T.; Jaafari, A.; Prakash, I.; Bui, D.T. A Novel Hybrid Intelligent Model of Support Vector Machines and the MultiBoost Ensemble for Landslide Susceptibility Modeling. *Bull. Eng. Geol. Environ.* **2019**, *78*, 2865–2886. [CrossRef]
31. Dou, J.; Paudel, U.; Oguchi, T.; Uchiyama, S.; Hayakawa, Y.S. Shallow and Deep-Seated Landslide Differentiation Using Support Vector Machines: A Case Study of the Chuetsu Area, Japan. *Terr. Atmos. Ocean. Sci.* **2015**, *26*, 227. [CrossRef]
32. Chen, W.; Li, X.; Wang, Y.; Chen, G.; Liu, S. Forested Landslide Detection Using LiDAR Data and the Random Forest Algorithm: A Case Study of the Three Gorges, China. *Remote Sens. Environ.* **2014**, *152*, 291–301. [CrossRef]
33. Selamat, S.N.; Abd Majid, N.; Mohd Taib, A. A Comparative Assessment of Sampling Ratios Using Artificial Neural Network (ANN) for Landslide Predictive Model in Langat River Basin, Selangor, Malaysia. *Sustainability* **2023**, *15*, 861. [CrossRef]
34. Wang, W.; Li, D.-Q.; Tang, X.-S.; Du, W. Seismic Fragility and Demand Hazard Analyses for Earth Slopes Incorporating Soil Property Variability. *Soil Dyn. Earthq. Eng.* **2023**, *173*, 108088. [CrossRef]
35. Liu, Y.; Li, J.; Lin, G. Seismic Performance of Advanced Three-Dimensional Base-Isolated Nuclear Structures in Complex-Layered Sites. *Eng. Struct.* **2023**, *289*, 116247. [CrossRef]
36. Liu, Q.-Y.; Li, D.-Q.; Tang, X.-S.; Du, W. Predictive Models for Seismic Source Parameters Based on Machine Learning and General Orthogonal Regression Approaches. *Bull. Seismol. Soc. Am.* **2023**, *113*, 2363–2376. [CrossRef]
37. Qin, S.; Guo, X.; Sun, J.; Qiao, S.; Zhang, L.; Yao, J.; Cheng, Q.; Zhang, Y. Landslide Detection from Open Satellite Imagery Using Distant Domain Transfer Learning. *Remote Sens.* **2021**, *13*, 3383. [CrossRef]
38. Shawky, O.A.; Hagag, A.; El-Dahshan, E.-S.A.; Ismail, M.A. Remote Sensing Image Scene Classification Using CNN-MLP with Data Augmentation. *Optik* **2020**, *221*, 165356. [CrossRef]
39. Rau, J.-Y.; Jhan, J.-P.; Rau, R.-J. Semiautomatic Object-Oriented Landslide Recognition Scheme from Multisensor Optical Imagery and DEM. *IEEE Trans. Geosci. Remote Sens.* **2014**, *52*, 1336–1349. [CrossRef]
40. Sameen, M.I.; Pradhan, B. Landslide Detection Using Residual Networks and the Fusion of Spectral and Topographic Information. *IEEE Access* **2019**, *7*, 114363–114373. [CrossRef]
41. Ghorbanzadeh, O.; Meena, S.R.; Blaschke, T.; Aryal, J. UAV-Based Slope Failure Detection Using Deep-Learning Convolutional Neural Networks. *Remote Sens.* **2019**, *11*, 2046. [CrossRef]
42. Yao, J.; Qin, S.; Qiao, S.; Che, W.; Chen, Y.; Su, G.; Miao, Q. Assessment of Landslide Susceptibility Combining Deep Learning with Semi-Supervised Learning in Jiaohe County, Jilin Province, China. *Appl. Sci.* **2020**, *10*, 5640. [CrossRef]
43. Yu, H.; Ma, Y.; Wang, L.; Zhai, Y.; Wang, X. A Landslide Intelligent Detection Method Based on CNN and RSG_R. In Proceedings of the 2017 IEEE International Conference on Mechatronics and Automation (ICMA), IEEE, Takamatsu, Japan, 6–9 August 2017; pp. 40–44.
44. Li, H.; He, Y.; Xu, Q.; Deng, J.; Li, W.; Wei, Y. Detection and Segmentation of Loess Landslides via Satellite Images: A Two-Phase Framework. *Landslides* **2022**, *19*, 673–686. [CrossRef]
45. Yun, L.; Zhang, X.; Zheng, Y.; Wang, D.; Hua, L. Enhance the Accuracy of Landslide Detection in UAV Images Using an Improved Mask R-CNN Model: A Case Study of Sanming, China. *Sensors* **2023**, *23*, 4287. [CrossRef] [PubMed]
46. Jin, Y.; Ou, O.; Wang, S.; Liu, Y.; Niu, H.; Leng, X. Landslide Detection Based on Efficient Residual Channel Attention Mechanism Network and Faster R-CNN. *ComSIS* **2023**, *20*, 893–910. [CrossRef]
47. Ghiasi, G.; Lin, T.-Y.; Le, Q.V. NAS-FPN: Learning Scalable Feature Pyramid Architecture for Object Detection. In Proceedings of the 2019 IEEE/CVF Conference on Computer Vision and Pattern Recognition (CVPR), IEEE, Long Beach, CA, USA, 15–20 June 2019; pp. 7029–7038.
48. Yasir, M.; Shanwei, L.; Mingming, X.; Hui, S.; Hossain, M.S.; Colak, A.T.I.; Wang, D.; Jianhua, W.; Dang, K.B. Multi-Scale Ship Target Detection Using SAR Images Based on Improved Yolov5. *Front. Mar. Sci.* **2023**, *9*, 1086140. [CrossRef]
49. Guo, H.; Yi, B.; Yao, Q.; Gao, P.; Li, H.; Sun, J.; Zhong, C. Identification of Landslides in Mountainous Area with the Combination of SBAS-InSAR and Yolo Model. *Sensors* **2022**, *22*, 6235. [CrossRef]
50. Ji, S.; Yu, D.; Shen, C.; Li, W.; Xu, Q. Landslide Detection from an Open Satellite Imagery and Digital Elevation Model Dataset Using Attention Boosted Convolutional Neural Networks. *Landslides* **2020**, *17*, 1337–1352. [CrossRef]
51. Li, B.; Li, J. Methods for Landslide Detection Based on Lightweight YOLOv4 Convolutional Neural Network. *Earth Sci. Inform.* **2022**, *15*, 765–775. [CrossRef]

52. Han, K.; Wang, Y.; Tian, Q.; Guo, J.; Xu, C.; Xu, C. GhostNet: More Features from Cheap Operations. In Proceedings of the 2020 IEEE/CVF Conference on Computer Vision and Pattern Recognition (CVPR), IEEE, Seattle, WA, USA, 13–19 June 2020; pp. 1577–1586.
53. Tan, M.; Pang, R.; Le, Q.V. EfficientDet: Scalable and Efficient Object Detection. In Proceedings of the IEEE/CVF Conference on Computer Vision and Pattern Recognition (CVPR), Seattle, WA, USA, 13–19 June 2020. [CrossRef]
54. Wang, Q.; Wu, B.; Zhu, P.; Li, P.; Zuo, W.; Hu, Q. ECA-Net: Efficient Channel Attention for Deep Convolutional Neural Networks. In Proceedings of the IEEE/CVF Conference on Computer Vision and Pattern Recognition, Seattle, WA, USA, 13–19 June 2020.
55. Mu, L.; Xian, L.; Li, L.; Liu, G.; Chen, M.; Zhang, W. YOLO-Crater Model for Small Crater Detection. *Remote Sens.* **2023**, *15*, 5040. [CrossRef]
56. Xu, W.; Ma, W.; Wang, S.; Gu, X.; Ni, B.; Cheng, W.; Feng, J.; Wang, Q.; Hu, M. Automatic Detection of VLF Tweek Signals Based on the YOLO Model. *Remote Sens.* **2023**, *15*, 5019. [CrossRef]